Selective Alcohol Oxidation

DOI: 10.1002/ange.201301868

Molecular Understanding of Reactivity and Selectivity for Methanol Oxidation at the Au/TiO_2 Interface**

Matteo Farnesi Camellone, Jianli Zhao, Lanying Jin, Yuemin Wang,* Martin Muhler, and Dominik Marx*

Gold-based catalysts have attracted great interest since the discovery of the exceptional catalytic activity of oxide-supported Au nanoparticles for a large number of oxidation reactions including low-temperature CO oxidation.[1] Despite extensive experimental and theoretical studies,[2–10] however, the origin of the high catalytic activity of Au/oxide catalysts has not been clarified. Many important issues such as the nature of the active sites and the activation of molecular oxygen are still under debate. In particular, little is known about the microscopic mechanism of complex reactions such as the selective oxidation of alcohol molecules on oxide-supported Au nanoparticles.[11]

Methanol (CH_3OH) is one of the most important industrial chemicals[12] and the selective oxidation of alcohols with oxygen is a key issue for the production of fine and specialty chemicals using "green" processes.[13] Herein, we present a surface-science study of the selective oxidation of methanol on a Au/TiO_2(110) model catalyst. The combined data, obtained from extensive density functional theory (DFT) calculations and experiments using high-resolution electron energy loss spectroscopy (HREELS) and thermal desorption spectroscopy (TDS), allow us to achieve an atomic-level understanding of the low-temperature oxidation of methanol with molecular oxygen to formaldehyde. We demonstrate herein that the high catalytic activity and selectivity of Au/TiO_2 originate from the presence of active interfacial sites, where the activation of molecular oxygen occurs through charge transfer from Au/TiO_2 forming $O_2^{\delta-}$ species. Oxygen activation is followed by the formation of a CH_3OH–O_2 intermediate, which undergoes oxidative dehydrogenation yielding CH_2O and H_2O. The latter is produced by recombination of hydroxy groups including hydrogen transfer from the Au cluster to an O atom at the perimeter site.

We first investigated the molecular reaction mechanism of the selective oxidation cycle of CH_3OH by O_2 on an Au_{11}/TiO_2(110) model surface by means of GGA + U calculations. It has been reported that very small unsupported and oxide-supported Au clusters (3–10 atoms) also show high catalytic activity towards CO oxidation and various organic reactions.[14] We have studied in detail the electronic structure of a set of Au_n clusters ($n = 11$–16) supported on TiO_2(110) (see Supporting Information, Section III.H). It was demonstrated that the charge of the activated $O_2^{\delta-}$ species is almost constant (Table S3), indicating that the behavior of Au_n nanoclusters of different size, shape, and morphology is qualitatively the same with respect to O_2 activation. Therefore, the Au_{11} model, although certainly being a simplification of nanometer-sized clusters on TiO_2(110), was shown to appropriately mimic the active sites located at the nanogold/oxide interface where the oxidation process takes place.[15]

As shown in Figure 1 A, a Au_{11} gold cluster was anchored at a single surface oxygen vacancy on the TiO_2(110) surface. Oxygen vacancies, which are always present on the rutile surface,[16] result in stable anchoring sites for Au adatoms. In the case of an isolated oxygen vacancy on the stoichiometric TiO_2(110) surface, the charge neutrality is maintained by the presence of two Ti^{3+} ions.[17] The stable binding of the Au_{11} cluster on an oxygen vacancy site entails a strong charge rearrangement at the gold/oxide contact (central panel in Figure 1). The bonding charge analysis reveals that charge transfer occurs from the Au_{11} cluster to the reduced oxide surface, thus leaving a reduced surface with three Ti^{3+} ions and a positively charged $Au_{11}^{\delta+}$ cluster.[18] This finding is further supported by the HREELS data as discussed below (see also Figure S1).

All the steps involved in the proposed mechanism for CH_3OH oxidation at the active Au_{11}/TiO_2(110) interface are depicted in Figure 1; all underlying data are compiled in the Supporting Information including connecting pathways and much additional analyses (Figure S3–S14). The catalytic cycle starts with the adsorption of an O_2 molecule at the interface on a dual perimeter site between the Au_{11} cluster and the TiO_2(110) surface (Figure 1 B) with a strong binding energy of −2.15 eV. The adsorbed O_2 molecule has an O–O bond length of 1.44 Å, close to the typical value for a peroxide (O_2^{2-}:

[*] Dr. M. Farnesi Camellone,[+] Prof. Dr. D. Marx
Lehrstuhl für Theoretische Chemie, Ruhr-Universität Bochum
44780 Bochum (Germany)
E-mail: matteo.farnesi@theochem.rub.de
Dr. J. Zhao,[+] L. Jin, Dr. Y. Wang
Lehrstuhl für Physikalische Chemie I and Lehrstuhl für Technische Chemie, Ruhr-Universität Bochum
44780 Bochum (Germany)
E-mail: wang@pc.rub.de
Prof. Dr. M. Muhler
Lehrstuhl für Technische Chemie, Ruhr-Universität Bochum
44780 Bochum (Germany)

[+] These authors contributed equally to this work.

[**] This work was supported by the Deutsche Forschungsgemeinschaft (DFG) within SFB 558 and by the Cluster of Excellence "RESOLV" (EXC 1069). Partial financial support from the Research Department "Interfacial Systems Chemistry" funded by RUB is gratefully acknowledged. Computational resources were provided by NIC (Jülich), Bovilab@RUB (Bochum), RV-NRW as well as PRACE (FERMI at Cineca).

Supporting information for this article is available on the WWW under http://dx.doi.org/10.1002/anie.201301868.

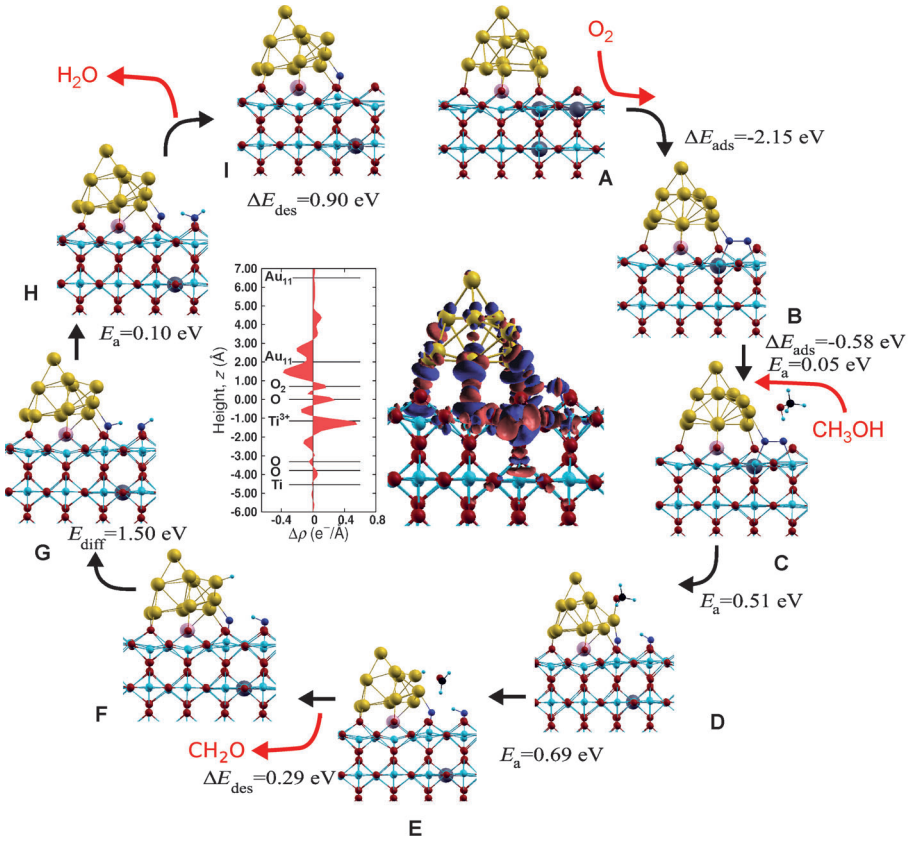

Figure 1. Selective methanol oxidation cycle proposed from calculations. The Au, Ti, O, and C atoms are shown in yellow, light blue, red, and black respectively, whereas the O_2 molecule adsorbed at the interface and H atoms of the CH_3OH molecule are shown in blue and small light blue spheres. The pink sphere represents the oxygen vacancy and the large dark spheres of the substrate show Ti^{3+} sites. ΔE_{ads}, E_a, ΔE_{des}, and E_{diff} refer to the adsorption energy, activation barrier, desorption energy, and diffusion barrier, respectively. The center of the Figure shows the calculated bonding charge $\Delta\rho$ for the Au_{11} cluster supported by the reduced TiO_2(110) surface in the presence of a preadsorbed O_2 molecule. Left: the bonding charge integrated in planes perpendicular to the surface and is plotted as a function of the height from the surface. Right: the bonding charge plotted at the value of 0.06 |e|Å^{-3}. Electron accumulation and depletion are represented by red and blue isosurfaces, respectively. Full details are provided in the Supporting Information.

1.49 Å). Each O atom binds to one surface Ti_{5c} atom. A close examination of the spin density, projected density of states (PDOS) and bonding charge reveals that upon O_2 adsorption the substrate degree of reduction changes: two of the three excess electrons originally populating Ti^{3+} sites of the titania surface are donated to the adsorbed O_2 molecule, which turns out to be a peroxide, while only one Ti^{3+} ion is present on the oxide support (see central panel in Figure 1). We note that the full catalytic cycle does not modify the degree of reduction of the oxide support, which indicates the presence of a single Ti^{3+} ion from the initial to the final state (Figure 1) of the proposed oxidation mechanism. This step is followed by the coadsorption of CH_3OH at the dual perimeter site on top of the O_2/TiO_2(110) (Figure 1C) with a binding energy of −0.58 eV. The adsorbed CH_3OH reacts directly with O_2/TiO_2(110) to form a CH_3OH-O_2 intermediate that is stabilized by interaction with the neighboring Au site right at the interface. As a result the O–O bond is weakened upon its interaction with CH_3OH, and dissociates with an activation energy of 0.05 eV to form Ti_{5c}-OH and Au-CH_3O (Figure 1D). This step involves the rupture of the O–O bond of the preadsorbed O_2 molecule, an H atom transfer from the methanol OH group to the surface O atom, and the binding of methoxy (CH_3O) to the neighboring Au atom (Figure S9). The O atom at the interface moves in the direction of the metal cluster, and the Au_{11} cluster rearranges its shape with an activation energy of 0.51 eV. A close examination of the PDOS along the reaction path reveals that the dissociation of the perimeter molecule is accompanied by a significant charge transfer (approximately 0.6 valence electrons) from the Au_{11} cluster to the dissociated O_2 molecule that stabilizes the Au-CH_3O intermediate (Figure S10).

The catalytic cycle proceeds through the formation of CH_2O from CH_3O by way of an additional oxidation. The calculated reaction path for the second oxidation step involves the donation of an H atom of the formed Au-CH_3O intermediate complex to a Au atom of the metal cluster. This step has an activation energy of 0.69 eV (Figure 1E). The supported Au_{11} metal cluster accepts an H atom from CH_3O, therefore acting as a hydrogen storage device. The formed CH_2O can easily desorb with a desorption energy of 0.29 eV (Figure 1F). The last part of the catalytic cycle concerns the formation of water. The H atom migrates on the gold cluster with a barrier of approximately 1.5 eV until it finds the activated O atom at the perimeter site to form an OH intermediate (Figure 1G), thereby changing its charge from close to 1.0 to about 0.5 |e|, i.e., transmuting from a H atom to a proton (Figure S13).

The hydroxy species thus formed can readily react with the neighboring OH group transferring the H atom with an activation energy of 0.10 eV, thereby leading to the formation of a H_2O molecule (Figure 1H). This H_2O molecule can desorb with a desorption energy of 0.90 eV (Figure 1I) thus completing the cycle and leaving behind an active O atom species at the interface. This step returns the catalyst surface to its initial working state, and the oxidation reaction can continue by adsorbing a second CH_3OH molecule at the Au perimeter site.

To examine the above microscopic mechanism for the high reactivity and selectivity of the Au/TiO_2 interface towards CH_3OH oxidation, we have carried out correspond-

ing experiments by means of HREELS and TDS. Following a method from the literature,[19] the supported Au nanoclusters were prepared by evaporating Au at 300 K onto an vacuum-annealed TiO_2(110) surface, which exposes approximately 10% of the surface oxygen vacancies.[20] The as-prepared sample was subsequently annealed at 750 K in vacuum to stabilize the Au clusters. The growth of Au clusters on rutile TiO_2(110) surfaces has been extensively studied by STM and non-contact AFM.[19] Table S1 shows the average size, height, and density of Au clusters on TiO_2(110) as a function of the Au coverage reported in previous studies.[2,19] After deposition of 0.2 monolayer (ML) Au on the reduced TiO_2(110) surface, the EELS spectrum shows a loss peak centered at 2.5 eV (Figure S1), which was assigned to the surface plasmon excitation of Au clusters.[21] This band was not detected at Au coverage less than 0.2 ML, indicating that the structural transition of Au adatoms from 2D to 3D configurations occurs at around 0.2 ML.[21] The loss at 0.8 eV originates from the excitation of shallow band gap states associated with Ti^{3+} sites at oxygen vacancies.[22] Its intensity increases at the initial deposition of Au (up to 0.2 ML) implying the formation of additional Ti^{3+} ions through charge transfer from Au to TiO_2 substrates as confirmed by the DFT calculations (Figure 1A). This band diminishes with further increasing Au coverage revealing that the Ti^{3+}-related excitation is significantly screened owing to the growth of 3D Au clusters at oxygen vacancy sites (Figure 1A).

The activation of molecular O_2 is a key issue for the low-temperature methanol oxidation on Au/TiO_2(110) and was studied by HREELS using CO exclusively as a probe molecule, which is extremely sensitive to the oxidation state of the Au species.[23] The raw spectrum of Au/TiO_2(110) is dominated by intense fundamental (358, 437, and 743 cm^{-1}) and multiple surface phonons (Figure 2A). The multiphonon-related losses have been successfully removed by Fourier deconvolution (Figure 2B), which allows us to reliably identify adsorbate-induced energy losses. In the absence of O_2 preadsorption, CO adsorption on Au/TiO_2(110) (0.4 ML Au) at 95 K exhibits two stretching bands at 2104 cm^{-1} and 2189 cm^{-1} (Figure 2C). The latter one is assigned to CO bound to coordinatively unsaturated Ti^{4+} sites on the "free" TiO_2(110) surface,[20] while the low-lying band at 2104 cm^{-1} is characteristic of the CO species bound to undercoordinated neutral Au sites at the Au/TiO_2 interface.[10,24] When the Au/TiO_2(110) sample is first exposed to O_2 and then to CO at 95 K, a new band emerges at 2136 cm^{-1}, indicating CO adsorption on the positively charged Au sites (Figure 2D). This band is further attributed to CO chemisorbed on low-coordinated Au sites in the presence of activated O_2 molecules at the interface, forming peroxo/superoxo-type $O_2^{\delta-}$-$Au^{\delta+}$-CO species.[24] The blue-shift in frequency compared to the 2104 cm^{-1} band originates from a charge transfer from Au/TiO_2 to molecular oxygen, which subsequently decreases the electron back-donation from Au to the CO $2\pi^*$ antibonding orbital and thus strengthens the internal C–O bond. The HREELS data reveal that O_2 activation occurs at the Au/TiO_2 interface by way of charge transfer yielding an $O_2^{\delta-}$ species, whereas no direct dissociation to atomic oxygen was detected at low temperatures, in excellent agreement with the calculated data (Figure 1B; Figure S3).

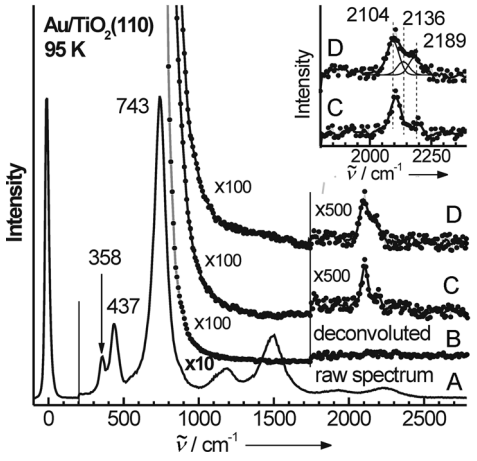

Figure 2. HREEL spectra of Au/TiO_2(110) obtained after CO adsorption at 95 K with and without O_2 preadsorption; note that CO is exclusively used as a probe molecule and not oxidized. A) The raw spectrum of clean Au/TiO_2 (0.4 ML Au). B) The spectrum obtained for clean Au/TiO_2 after Fourier deconvolution to remove the intense multiple surface phonons, C) deconvoluted spectrum for CO adsorption on Au/TiO_2 at 95 K, and D) deconvoluted spectrum for CO adsorption subsequent to O_2 adsorption on Au/TiO_2 at 95 K.

The TDS results provide direct evidence for the selective oxidation of CH_3OH on Au/TiO_2(110). For all the TDS experiments, the heating temperature was limited below 730 K, at which Au cluster sintering does not occur,[19] as confirmed by the reproducibility of the TD spectra. The corresponding TD spectra for CH_3OH, CH_2O, and H_2O are presented in Figure 3A–C. The TDS data reveal the occurrence of a well-known high-temperature reaction channel (> 600 K) forming CH_2O for both pure and Au-decorated TiO_2(110) surfaces (Figure 3B,D). The production of CH_2O is accompanied by CH_3OH desorption. This reaction is independent of the presence of Au nanoparticles and occurs on the TiO_2(110) surface, on which the methoxy groups undergo disproportionation to form CH_3OH and CH_2O.[25] In stark contrast, we focused on the role played by the Au/TiO_2 interface and demonstrated that a low-temperature channel for selective CH_3OH oxidation to CH_2O opens on Au/TiO_2.

In the case of the Au/TiO_2(110) surface (with 0.4 ML Au deposition) being solely exposed to CH_3OH at 95 K, only the desorption of CH_3OH is observed indicating that no low-temperature methanol oxidation occurs in the absence of coadsorbed oxygen at the Au/TiO_2 interface. The CH_3OH desorption leads to a dominating peak at 297 K, which is assigned to the CH_3OH species bound to Ti^{4+} sites on TiO_2(110) (Figure S2).[25] In addition, a shoulder around 400 K is resolved at the higher temperature side. This peak is related to CH_3OH adsorbed at the Au/TiO_2 interface as supported by the experimental and theoretical results discussed below. By assuming a pre-exponential factor of 10^{13} s^{-1} and first-order kinetics, the activation energies for CH_3OH desorption from the TiO_2(110) surface and Au/TiO_2(110) interface are estimated to be 0.88 eV and 1.21 eV, respectively, which are in agreement with the calculated values (0.86 eV and 1.13 eV; Figure S15 and Table S2).

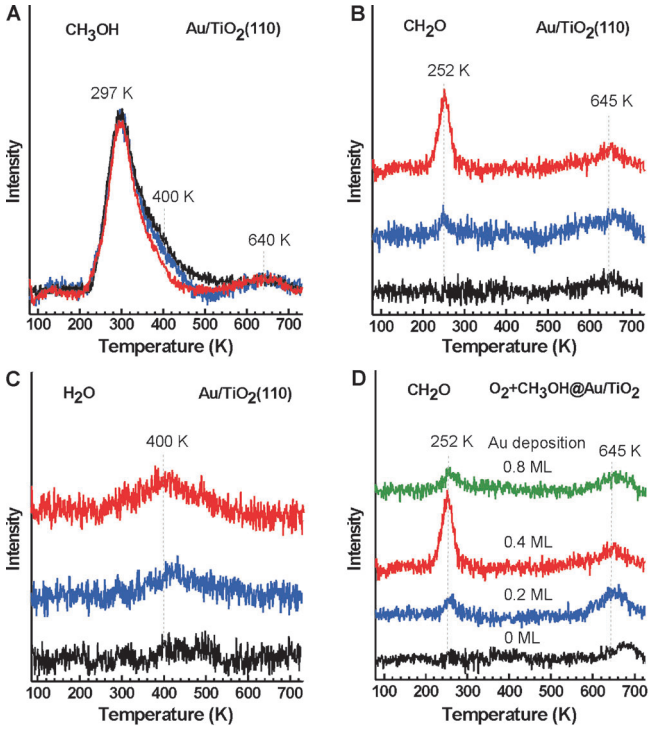

Figure 3. TD spectra of $Au/TiO_2(110)$ obtained after adsorption of CH_3OH and O_2 at 95 K. The desorption data were recorded for the following species: A) CH_3OH, B) CH_2O, C) H_2O. The spectra in (A), (B), and (C) were obtained after CH_3OH adsorption on $Au/TiO_2(110)$ (black), O_2 adsorption subsequent to CH_3OH adsorption on $Au/TiO_2(110)$ (blue), and CH_3OH adsorption subsequent to O_2 adsorption on $Au/TiO_2(110)$ (red) at 95 K. d) CH_2O desorption from $Au/TiO_2(110)$ as a function of Au coverage obtained after CH_3OH adsorption subsequent to O_2 adsorption on $Au/TiO_2(110)$ at 95 K. The heating rate was 1.5 $K s^{-1}$.

For the sequential adsorption of first O_2 and then CH_3OH on $Au/TiO_2(110)$ at 95 K, the selective oxidation of CH_3OH to formaldehyde and water takes place at the interface between Au and TiO_2 upon heating to higher temperatures, as clearly confirmed by the appearance of a sharp desorption peak of CH_2O at 252 K and a broad H_2O peak centered around 400 K (Figure 3 B,C). The formation of CH_2O and H_2O is accompanied by the consumption of CH_3OH species bound to the Au/TiO_2 interface, while the intensity of the TiO_2-related CH_3OH peak at 297 K remains unchanged (Figure 3 A). Importantly, no other products such as H_2, CO, CO_2, and HCOOH are observed in the TD spectra revealing that the Au/TiO_2 interface exhibits both high catalytic activity and selectivity for formaldehyde production.

Interestingly, when oxygen is adsorbed subsequent to CH_3OH adsorption on $Au/TiO_2(110)$, the formation of CH_2O at 252 K is dramatically reduced (Figure 3), and water desorption from the interface also diminishes accordingly. These findings indicate that the preadsorption of O_2 is crucial for the low-temperature selective oxidation of CH_3OH at the Au/TiO_2 interface, in line with the DFT mechanism (Figure 1 C,D; Figure S9). Given that the desorption of CH_2O formed through CH_3OH oxidation is controlled by the reaction, the peak at 252 K yields an activation energy of 0.68 eV for CH_2O formation, in excellent agreement with the calculated result (0.69 eV, Figure 1 E,F; Figure S12). In addition, the broad H_2O desorption peak at a higher temperature range is indicative of the recombination of hydroxy species formed by CH_3OH oxidation in accord with the theoretical reaction scenario (Figure 1 H,I; Figure S14). Furthermore, the desorption temperature centered at 400 K supports the relatively high diffusion barrier of hydrogen transfer from the Au cluster to an O atom at the perimeter site thus forming OH species (1.1 eV; Figure 1 G; Figure S13).

The impact of Au coverage on methanol oxidation at the Au/TiO_2 interface was also investigated. As shown in Figure 3 D, no CH_2O desorption is observed at 252 K on the pure $TiO_2(110)$ surface. The CH_2O production increases with increasing Au coverage and reaches a maximum at 0.4 ML. Further increasing the Au coverage to 0.8 ML leads to a significant decrease of the CH_2O yield. The TDS data reveal that 0.4 ML is the optimum coverage of Au to achieve the maximum concentration of interfacial sites. This coverage of Au clusters corresponds to an average particle size of 3–3.5 nm (Table S1).[19] It has been reported that supported Au nanoparticles of this size are the most active ones for CO oxidation.[2,10] In addition, it has been proposed that this reaction occurs at dual perimeter sites between Au and TiO_2.[10] The population of interfacial sites is lowered at higher Au coverage owing to the formation of larger Au clusters (Table S1). These findings provide further evidence for the crucial role of the Au/TiO_2 interface in low-temperature methanol oxidation.

Overall, our experimental and theoretical results demonstrate consistently that the interfacial sites between Au and TiO_2 open a low-temperature reaction channel for the selective oxidation of methanol to formaldehyde and water. Detailed insights into the fundamental mechanism involved in this complex reaction have been obtained, which will impact the design of efficient Au-based catalysts with high reactivity and selectivity in particular for low-temperature alcohol oxidation.

Experimental Section

The first-principles density functional theory (DFT) calculations have been performed using the Car–Parrinello Molecular Dynamics (CPMD) and the Quantum Espresso codes. All the calculations have been performed using spin-polarized GGA + U, Perdew–Burke–Ernzerhof exchange-correlation functional (PBE). The spin-polarized Kohn–Sham equations were solved in the plane-wave and pseudopotential framework using Vanderbilt's ultrasoft pseudopotential with a cutoff of 25 Ry using the Γ point. In line with our previous work, we made use of the LDA + U implementation and a value of $U = 4.2$ eV.

The HREELS and TDS experiments were performed in a ultra-high vacuum (UHV) apparatus consisting of two chambers connected by a valve. The base pressure was 5×10^{-11} mbar. The upper chamber was equipped with LEED optics and a quadrupole mass spectrometer used to perform TDS experiments. The lower chamber housed a HREEL spectrometer (Delta 0.5, SPECS, Germany) with a straight-through energy resolution of 1 meV. The $TiO_2(110)$ single crystal was cleaned by repeated cycles of sputtering (1 keV Ar^+, 30 min) and annealing (850 K, 5 min). Typically, about two cycles were followed by one cycle with annealing in an ambient oxygen

environment. The reduced surface was obtained by annealing to 900 K in vacuum. The gold nanoparticles were deposited onto TiO_2(110) using an electron beam evaporator (EBE-4, Specs). A quartz crystal microbalance (QCM) was used to measure the coverage of gold deposited onto the substrate. The background pressure was less than 1×10^{-9} mbar during Au deposition. After deposition, the samples were annealed at 750 K in vacuum for 2 min to ripen and stabilize the Au nanoparticles.[19]

Received: March 5, 2013
Published online: April 15, 2013

Keywords: density functional calculations · gold nanoparticles · methanol · TiO_2 · vibrational spectroscopy

[1] a) M. Haruta, T. Kobayashi, H. Sano, N. Yamada, *Chem. Lett.* **1987**, 405 – 408; b) M. Haruta, *Chem. Rec.* **2003**, *3*, 75 – 87.
[2] a) M. Valden, X. Lai, D. W. Goodman, *Science* **1998**, *281*, 1647 – 1650; b) M. S. Chen, D. W. Goodman, *Science* **2004**, *306*, 252 – 255.
[3] B. K. Min, C. M. Friend, *Chem. Rev.* **2007**, *107*, 2709 – 2724.
[4] R. Meyer, C. Lemire, S. K. Shaikhutdinov, H. J. Freund, *Gold Bull.* **2004**, *37*, 72 – 124.
[5] I. N. Remediakis, N. Lopez, J. K. Norskov, *Angew. Chem.* **2005**, *117*, 1858 – 1860; *Angew. Chem. Int. Ed.* **2005**, *44*, 1824 – 1826.
[6] A. S. K. Hashmi, G. J. Hutchings, *Angew. Chem.* **2006**, *118*, 8064 – 8105; *Angew. Chem. Int. Ed.* **2006**, *45*, 7896 – 7936.
[7] B. Yoon, H. Häkkinen, U. Landman, A. Wörz, J. M. Antonietti, S. Abbet, S. K. Judai, U. Heiz, *Science* **2005**, *307*, 403 – 407.
[8] a) M. M. Schubert, S. Hackenberg, A. C. van Veen, M. Muhler, V. Plzak, R. J. Behm, *J. Catal.* **2001**, *197*, 113 – 122; b) D. Widmann, R. J. Behm, *Angew. Chem.* **2011**, *123*, 10424 – 10428; *Angew. Chem. Int. Ed.* **2011**, *50*, 10241 – 10245.
[9] C. Jia, J. Liu, H. Bongard, F. Schüth, *J. Am. Chem. Soc.* **2010**, *132*, 1520 – 1522.
[10] I. X. Green, W. Tang, M. Neurock, J. T. Yates, Jr., *Science* **2011**, *333*, 736 – 739.
[11] a) S. Biella, M. Rossi, *Chem. Commun.* **2003**, 378 – 379; b) D. I. Enache, J. K. Edwards, P. Landon, B. Solsona-Espriu, A. F. Carley, A. A. Herzing, M. Watanabe, C. J. Kiely, D. W. Knight, G. J. Hutchings, *Science* **2006**, *311*, 362 – 365; c) A. Corma, H. A. García, *Chem. Soc. Rev.* **2008**, *37*, 2096 – 2126.
[12] a) G. A. Olah, A. Goeppert, G. K. Surya Prakash, Wiley-VCH, Weinheim, **2006**; b) M. Behrens, F. Studt, I. Kasatkin, S. Kühl, M. Hävecker, F. Abild-Pedersen, S. Zander, F. Girgsdies, P. Kurr, B. L. Kniep, M. Tovar, R. W. Fisher, J. K. Nørskov, R. Schlögl, *Science* **2012**, *336*, 893 – 897.
[13] a) I. E. Markó, P. R. Giles, M. Tsukazaki, S. M. Brown, C. J. Urch, *Science* **1996**, *274*, 2044 – 2046; b) T. Mallat, A. Baiker, *Chem. Rev.* **2004**, *104*, 3037 – 3058; c) M. D. Hughes, Y. J. Xu, P. Jenkins, P. McMorn, P. Landon, D. I. Enache, A. F. Carley, G. A. Attard, G. J. Hutchings, F. King, E. H. Stitt, P. Johnston, K. Griffin, C. J. Kiely, *Nature* **2005**, *437*, 1132 – 1135.
[14] a) S. Lee, C. Fan, T. Wu, S. L. Anderson, *J. Am. Chem. Soc.* **2004**, *126*, 5682 – 5683; b) A. A. Herzing, C. J. Kiely1, A. F. Carley, P. Landon, G. J. Hutchings, *Science* **2008**, *321*, 1331 – 1335; c) J. Oliver-Meseguer, J. R. Cabrero-Antonino, I. Domínguez, A. Leyva-Pérez, A. Corma, *Science* **2012**, *338*, 1452 – 1455.
[15] a) J. G. Wang, B. Hammer, *Phys. Rev. Lett.* **2006**, *97*, 136107; b) H. Y. Kim, M. Lee, G. Henkelman, *J. Am. Chem. Soc.* **2012**, *134*, 1560 – 1570.
[16] U. Diebold, *Surf. Sci. Rep.* **2003**, *48*, 53 – 229.
[17] a) M. V. Ganduglia-Pirovano, A. Hofmann, J. Sauer, *Surf. Sci. Rep.* **2007**, *62*, 219 – 270; b) P. Kowalski, M. Farnesi Camellone, N. N. Nair, B. Meyer, D. Marx, *Phys. Rev. Lett.* **2010**, *105*, 146405.
[18] a) M. Farnesi Camellone, P. M. Kowalski, D. Marx, *Phys. Rev. B* **2011**, *84*, 035413; b) D. Matthey, J. G. Wang, S. Wendt, J. Matthiesen, R. Schaub, E. Lægsgaard, B. Hammer, F. Besenbacher, *Science* **2007**, *315*, 1692 – 1696; c) S. Chrétien, H. Metiu, *J. Chem. Phys.* **2007**, *127*, 244707.
[19] a) X. Lai, T. P. St. Clair, M. Valden, D. W. Goodman, *Prog. Surf. Sci.* **1998**, *59*, 25 – 52; b) X. Lai, D. W. Goodman, *J. Mol. Catal. A* **2000**, *162*, 33 – 50; c) C. E. J. Mitchell, A. Howard, M. Carney, R. G. Egdell, *Surf. Sci.* **2001**, *490*, 196 – 210; d) A. K. Santra, A. Kolmakov, F. Yang, D. W. Goodman, *Jpn. J. Appl. Phys.* **2003**, *42*, 4795 – 4798; e) S. Kielbassa, M. Kinne, R. J. Behm, *J. Phys. Chem. B* **2004**, *108*, 19184 – 19190; f) T. Minato, T. Susaki, S. Shiraki, H. S. Kato, M. Kawai, K. Aika, *Surf. Sci.* **2004**, *566*, 1012 – 1017.
[20] M. Xu, H. Noei, K. Fink, M. Muhler, Y. Wang, C. Wöll, *Angew. Chem.* **2012**, *124*, 4810 – 4813; *Angew. Chem. Int. Ed.* **2012**, *51*, 4731 – 4734.
[21] Q. Guo, K. Luo, K. A. Davis, D. W. Goodman, *Surf. Interface Anal.* **2001**, *32*, 161 – 165.
[22] M. A. Henderson, W. S. Epling, C. H. F. Peden, C. L. Perkins, *J. Phys. Chem. B* **2003**, *107*, 534 – 545.
[23] a) M. A. Brown, F. Ringleb, Y. Fujimori, M. Sterrer, H. J. Freund, G. Preda, G. Pacchioni, *J. Phys. Chem. C* **2011**, *115*, 10114 – 10124; b) H. Noei, A. Birkner, K. Merz, M. Muhler, Y. Wang, *J. Phys. Chem. C* **2012**, *116*, 11181 – 11188.
[24] F. Boccuzzi, A. Chiorino, M. Manzoli, M. Haruta, *J. Catal.* **2001**, *202*, 256 – 267.
[25] a) M. A. Henderson, S. Otero-Tapia, M. E. Castro, *Faraday Discuss.* **1999**, *114*, 313 – 329; b) E. Farfan-Arribas, R. J. Madix, *Surf. Sci.* **2003**, *544*, 241 – 260.

